

**TURBULENT BLUFF-BODY FLAMES CLOSE TO  
STABILITY LIMITS REVEALED BY COUPLING OF  
HIGH SPEED OPTICAL DIAGNOSTICS**

Nelson Valdez, David Honoré, Corine Lacour, Bertrand Lecordier, Armelle  
Cessou

► **To cite this version:**

Nelson Valdez, David Honoré, Corine Lacour, Bertrand Lecordier, Armelle Cessou. TURBULENT BLUFF-BODY FLAMES CLOSE TO STABILITY LIMITS REVEALED BY COUPLING OF HIGH SPEED OPTICAL DIAGNOSTICS. European Combustion Meeting 2019, Apr 2019, Lisbon, Portugal. hal-02110925

**HAL Id: hal-02110925**

**<https://hal.archives-ouvertes.fr/hal-02110925>**

Submitted on 25 Apr 2019

**HAL** is a multi-disciplinary open access archive for the deposit and dissemination of scientific research documents, whether they are published or not. The documents may come from teaching and research institutions in France or abroad, or from public or private research centers.

L'archive ouverte pluridisciplinaire **HAL**, est destinée au dépôt et à la diffusion de documents scientifiques de niveau recherche, publiés ou non, émanant des établissements d'enseignement et de recherche français ou étrangers, des laboratoires publics ou privés.

# TURBULENT BLUFF-BODY FLAMES CLOSE TO STABILITY LIMITS REVEALED BY COUPLING OF HIGH SPEED OPTICAL DIAGNOSTICS

Nelson VALDEZ<sup>\*</sup>, David HONORE, Corine LACOUR, Bertrand LECORDIER, Armelle CESSOU

Normandie Univ, INSA Rouen, UNIROUEN, CNRS, CORIA, 76000 Rouen, France

## Abstract

The understanding of flame stabilization is a requirement for the development of innovative combustion regimes associated to low pollutant emissions and high efficiency. Bluff-body burners are well adapted for the stabilization of turbulent non-premixed flames near extinction limit. In the present work, the stabilization mechanisms involved in turbulent bluff-body flames are investigated by means of time-resolved optical diagnostics. High-Rate Particle Image Velocimetry (HR-PIV) is coupled simultaneously to High-Rate flame imaging in order to point out the correlation between the aerodynamic fields and the flame structures from images time series. A periodic ejection of burning pockets is observed from the recirculation zone established at the burner exit to the base of the main lifted flame. The characteristic frequencies are determined by extracting local velocities and flame emission with time. This periodic behaviour is correlated to the intermittency of the aerodynamic structures. These results provide a better understanding of the physical phenomena controlling the stabilization of this turbulent flame.

## Introduction

The improvement of combustion is still an important issue for the scientific community today. The requirement of the increase of efficiency and the pollutants reduction become an essential task, which imposes constraints and new physical problems for industrial burner manufacturers and furnaces users. Recent innovative combustion regimes with low pollutants emissions and high energy efficiency usually operate with turbulent flames close to limits of stability. It is then essential to have a deeper understanding of physical phenomena leading to flame stabilization in order to be able to master, control and enhance it.

Bluff-body configuration is well adapted for the stabilization of non-premixed flames in industrial applications, such as in gas turbines, ramjets and furnaces [1, 2]. The internal recirculation zone generated by the wake effect of the flow downstream of the bluff-body induces then the partially mixing of the fuel with oxidant. Caetano et al. and Masri et al. in their studies have observed two vortices in the recirculation zone: the inner recirculation vortex (or central jet driven) is located on the side of the fuel jet whereas the outer recirculation vortex (or air driven) is located at the edge of the recirculation zone, radially further away from the axis, in contact with the annular flow [3, 4]. Trapping of high-temperature combustion products in the recirculation zone brings the necessary heat for the stabilization of the flame [5-7].

The understanding of these stabilization phenomena in turbulent flames requires the ability to perform time-resolved measurements by use of high-rate optical and laser diagnostics. Morales et al. have

investigated experimentally lean flame blowout within a high-speed combustor to analyze the temporal extinction dynamics of turbulent premixed bluff-body flames [8]. The lean blowout process is captured temporally using simultaneous high-speed PIV and CH\*chemiluminescence. The evolution of the flame structure, flow field, and the resulting flame strain rate are analyzed throughout extinction. This study shows that global extinction can be predicted with a Karlovitz number, only after  $Ka$  exceeds 2.4 does the flame structure undergo noticeable necking and the flame begins to extinguish. Similarly in his work, Mokaddem used the flame imaging technique with a high acquisition rate (2000 images/s), to visualize the displacement of burning pockets of the Bluff-Body burner flame [7]. Their results show that these structures provide the heat and reactive species necessary for the downstream jet-like flame stabilization. The flame-vortex dynamics are found to be the main driving mechanism of flame extinction. Furthermore, Tong et al. have studied flame stabilization mechanisms of a turbulent flame stabilized by combinations of swirl flow and bluff-body [2]. The flow is captured using high-speed PIV, while the flame structures were visualized by high-speed CH<sub>2</sub>O PLIF and CH\* chemiluminescence. The global CO emissions from the flames were collected as well. They have found that the position of the outer recirculation zone is affected by the size of the bluff-body and the swirl strength. Also the recirculation zone determines the flame structures and the global CO emission levels. With a larger bluff-body, the air driven recirculation zone is located closer to the burner exit. The stabilization phenomenon is then controlled

---

<sup>\*</sup> Corresponding author: [nelson.valdez-paulino@coria.fr](mailto:nelson.valdez-paulino@coria.fr)  
Proceedings of the European Combustion Meeting 2019

by heat transfers occurring in the recirculation zone. However, even if heat transfers play an important role, they cannot be separated from the wake aerodynamics, especially in the case of non-premixed flames, for which fluid mechanics will manage reactants residence times in the recirculation zone and thus influence the mixing process [9, 10].

In this configuration, the modes of stabilization of turbulent flames consist usually in unsteady phenomena in the internal recirculation zone which are complex and still poorly understood. Ejection of burning pockets from recirculation zone may be periodic and could be correlated with the complex aerodynamic structure of the flow induced by the bluff-body and the periodic burning pockets ejection. In the present study aerodynamics and flame structures are correlated for a turbulent non-premixed methane-air flame stabilized on a bluff-body burner, by means of coupling HR PIV with flame imaging.

## 1. Experimental setup

### 1.1. Burner configuration

To investigate turbulent flame stabilization, a bluff-body burner consisting of two coaxial jets is set up. The experimental device is presented in Fig. 1. Methane is injected in the central jet ( $D_c=7.5$  mm) while air is injected in the annular one ( $D_a=55$  mm). The  $D_b=48$  mm-dia. bluff-body induces a large blocking ratio of 0.83.

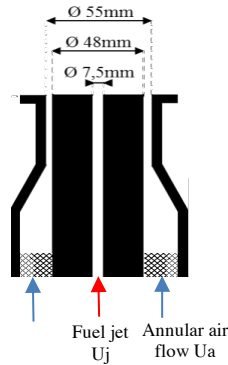


Figure 1. Bluff-body burner.

### 1.2. Stability diagram

The stability diagram is established as a first step, it provides information on the operating range of the burner as well as on the overall structures of the flames stabilized on this burner. Fig. 2 shows the stability diagram of the bluff-body burner. It has been established by fixing a constant methane jet velocity and increasing the annular air velocity up to the extinction limits.

Several structures of the flames have been identified in the stability diagram and their global topologies are presented in Fig. 3. Flame (a), occurring for low air velocity is dominated by the central jet of fuel. Flame (b) represents a transition flame characterized by the apparition of a small recirculation

zone. Flame (c) reveals a blue cone with a base consisting of a laminar blue ring lifted from the burner exit. Both are broad and surround a laminar soot diffusion core. In flame (d) for low methane jet velocity and large annular air velocity, the fuel is mixed with the recirculating air and the whole is burnt before leaving the recirculation area. The flame structure (e) shows a flame leading edge anchored to the aerodynamic internal recirculation zone induced by the bluff-body wake. A jet-like flame is stabilized downstream of this leading edge. This flame structure, especially investigated in this work, is particularly of interest because it corresponds to typical operating conditions in practical burners and it may present intermittent phenomena. Flame (f) represents a lifted flame completely detached from the burner nozzle when the jet velocity of the flame is over a critical value, around 22 m/s in the present case. Upper limit of the stability diagram corresponds to the limit of flame blow-out (g).

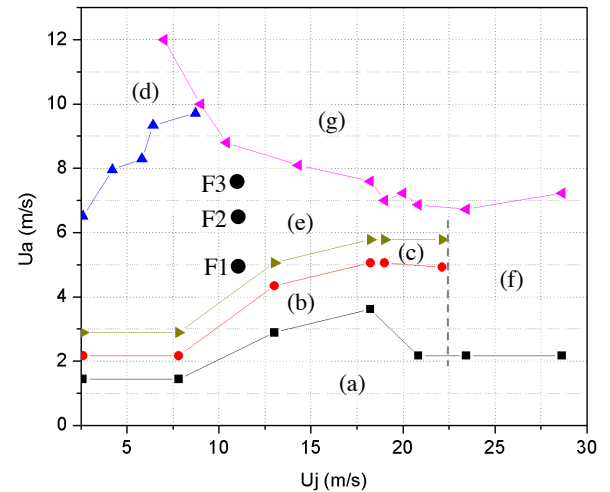


Figure 2. Stability diagram: (a) cylindrical flame, (b) Transition flame, (c) Ring laminar flame, (d) Recirculating flame, (e) long turbulent attached flame, (f) Lifted flame, (g) Extinction. F1, F2 and F3 refer to operating conditions studied in details in the present

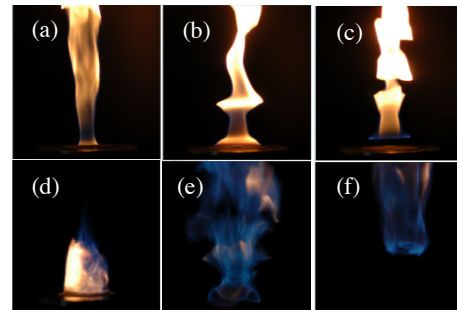


Figure 3. Direct flame visualizations of the different combustion regimes.

work.

The operating conditions chosen for detailed characterization are established for a constant central

methane jet velocity ( $U=10.9$  m/s) and a variation of annular air velocity from  $U= 5.0$  to  $7.5$  m/s (Fig.2). Three “type (e)” flames are retained from a fully stabilized turbulent flame (F1) chosen as reference case to a flame close to the blow-out limit (F3) passing by another stable flame (F2). The corresponding operating conditions are presented in Table 1. The air flow Reynolds number  $Re_a$  is determined from the diameter of the bluff-body.

$U_j$ (m/s)	$Re_a$	$U_a$ (m/s)	$Re_a$	Flame
10.9	4885	5.0	16170	F1
10.9	4885	6.5	21024	F2
10.9	4885	7.5	24258	F3

**Table 1.** Operating conditions.

### 1.3. Optical diagnostics

The flow and flame structures are characterized by means of the coupling of high-rate PIV and time-resolved flame emission.

The HR-PIV setup consists of a double cavity Nd:Ylf laser (Dual-DARWIN-527100-M 30 mJ @ 527 nm). A vertical laser sheet is formed by combining a spherical lens ( $f = 1000\text{mm}$ ) and a cylindrical lens ( $f = 40\text{mm}$ ). The laser sheet is carefully adjusted to cross the median plane of the burner and its height is around 130 mm from the burner exit. The air and methane flows are independently seeded with solid zirconium oxide particles ( $5\mu\text{m}$  mean diameter) that survives the reaction zone (melting point of 2988 K). The reactants flowrates are controlled by mass flowmeters before flowing into the two fluidized beds seeding machines, allowing a careful and balanced adjustment of the particle density in each flow. Particle images are collected with a Phantom V25 CMOS camera ( $1280 \times 800$  pixels) equipped with a Nikkor 50mm ( $f/1.2$ ) and an interferential filter (centered on 527 nm). The measurement analysis area corresponds to a surface of  $120\text{mm} \times 150\text{mm}$  and the spatial resolution is  $93 \mu\text{m}/\text{pix}$ . The acquisition rate is fixed to 5 kHz. Velocity fields are obtained by a laboratory property PIV cross-correlation algorithm [11, 12]. A multi-pass subpixel shift correlation algorithm has been used. Initial pass is computed with an interrogation window size of  $16 \times 32$  pixels the final pass is fixed to  $8 \times 32$  pixels ( $0.74 \times 2.96\text{mm}^2$ ) with an overlap of  $50 \times 25\%$ . Intermediate filtering is based on a minimum value of Signal to Noise Ratio (SNR) and a median filter that rejects most of non-valid vectors and resulting in instantaneous fields with more than 95 % validated vectors.

The flame emission is collected through a Phantom V9 high-speed camera equipped with a double stage HiCATT 25 intensifier and a UV Cerco 105 mm lens ( $f/2.8$ ). An acquisition rate at 1 kHz with a gate of  $140 \mu\text{s}$  are chosen as the best compromise between signal level and time integration. The spatial resolution is  $113.6 \mu\text{m}/\text{pix}$ .

The high speed camera and intensifier are synchronized with the PIV laser and camera by means of a BNC-555 delay generator. Simultaneous time series of 1.5 seconds duration are recorded.

## 2. Aerodynamic characterization

The mean velocity field obtained for F1 flame is presented in Fig. 4. The average of 7500 instantaneous velocity fields ensures the convergence of the statistics.

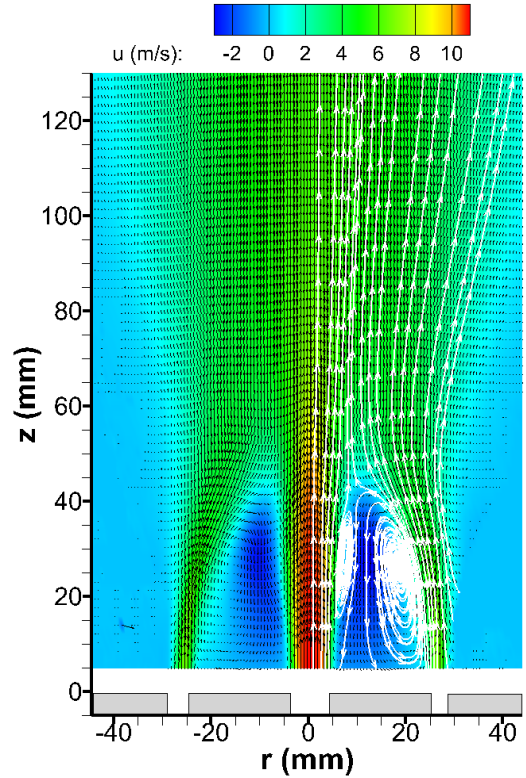


**Figure 4.** Time averaged axial velocity field and mean streamlines, F1 flame.

Three regions can be distinguished in the flow. A first zone corresponds to the recirculation zone from the nozzle of the burner up to  $z = 40\text{mm}$ . In a second zone, between  $40$  mm and  $60$  mm, the air flow streamlines converge towards the centerline. The last zone located from  $60$  mm and downstream corresponds to the development of the whole flow as a jet.

The recirculation zone is of particular importance in such a configuration. It is established between the central methane jet and the annular air jet and is defined by two toroidal vortices. The first large centripetal vortex is piloted by air jet and the second, smaller and centrifugal is piloted by the methane jet. These two vortices can be found in various non-premixed bluff-body configurations whatever the blocking ratio, the momentum ratio, in confined or free flow [5, 8]. The stagnation point gives the downstream boundary of the recirculation zone (respectively at  $r = -8$  mm  $z = 40$  mm and  $r = 9$  mm  $z = 41$  mm).

mm on left and right sides), which is close to the bluff-body diameter.

### 3. Mean structure of the flame

The global morphology of the flame is obtained by OH\* chemiluminescence imaging. The signal is collected with an ICCD Princeton PI-MAX 4 camera with a 16-bit 1024×1024 px<sup>2</sup> sensor, equipped with a UV Sodem 105 mm lens (f/2.8) and a UG11 filter covering a 180×180 mm<sup>2</sup> domain (175 μm/px). A mean image obtained from 1000 single shot images (60 μs) is presented in Fig.5 for flame F1. From the burner exit, the mean reaction zone is located at the external border of the recirculation zone. Downstream in the flow, a mean jet-like flame is developed in continuity. Similar topology of the mean flame is observed for the other operating conditions (F2 and F3) with higher lift-off location of the flame in the recirculation zone.

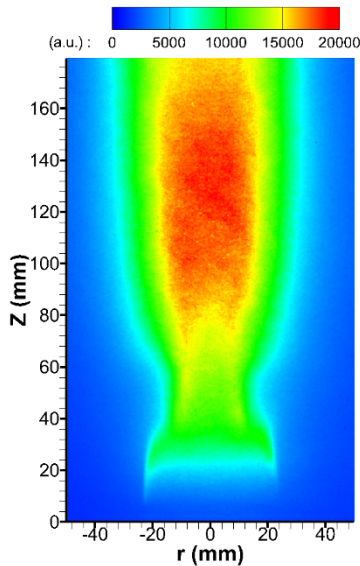


**Figure 5.** Averaged OH\* chemiluminescence image from 1000 images, F1 flame.

Short-gated high-rate flame imaging is then used to get the turbulent flame structures and follow their evolution with time. Fig. 6 shows a series of eighteen flames images, each separated with 2 ms. In the recirculation zone, the leading edge of the flame is seen to be lifted and anchored at the inner side of the annular air jet, as also noticed on the picture presented in Fig. 3.

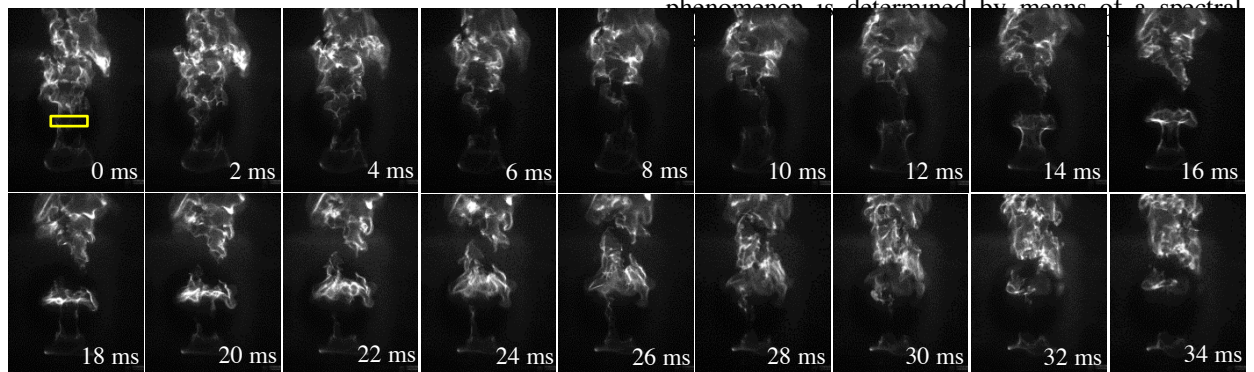


**Figure 6.** A short sequence of one time series of 1 kHz images of the F1 flame (1 image over 2 is shown).

Downstream, large regions of flame extinction are observed between the recirculation zone and the main trailing flame. On the eighteen successive flame images, a reactive pocket is detached from the flame leading edge, ejected from the recirculation zone and then transported by the flow, till the downstream zone of the depleted jet flame which is re-ignited by the flame pocket. This seems to be an intermittent phenomenon more or less observable depending on the operating conditions.

### 4. Frequency determination of reactive pockets ejection

The presence of a characteristic frequency of the reactive kernels ejection is evaluated by post-processing of the flame emission images. Firstly, a standard deviation (std) image is obtained by subtracting the mean image on each instantaneous image of the time series. Then, the flame intensity is averaged in a specific area of 8 × 3.4 mm<sup>2</sup> (see Fig. 6, yellow area) for each std image. This area is centered on point r=0 mm, z= 50 mm on top of the recirculation zone.

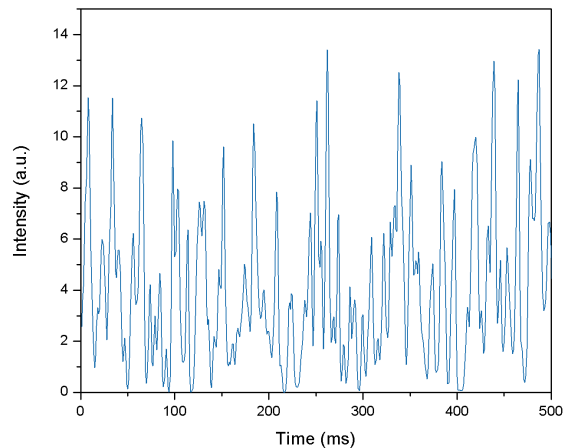


**Figure 7.** Temporal follow-up of the average flame intensity, F2 flame.

A temporal evolution of F2 flame emission intensity as a function of time is shown in Fig. 7. The evolution of the grey level extracted from the analysis window clearly shows the highly fluctuating nature of the turbulent flame.

The characteristic frequency of a potential intermittent phenomenon is determined by means of a spectral

profile obtained for the F2 flame is presented in Fig. 8. One clearly sees the presence of a peak which allows to quantify the frequency characterizing the periodic kernel ejection. This procedure is applied on three time series for each studied flame and the characteristic frequencies are gathered in Table 2.

Similar results are obtained for other position and size of the analysis window on the top of the recirculation zone. A typical frequency of 70 Hz is determined for F1 flame and a larger value of 90 Hz is observed for F2 flame due to the increase of air flowrate. This demonstrates the intermittent feature of the ejection of burning pockets from the recirculation zone to the main flame base. The periodic event seems to be correlated to the air flow aerodynamics since its characteristic frequency increases with air velocity. In the case of flame F3, close to the extinction limits, the flame structure do no more exhibits any periodic behavior as no characteristic frequency could be extracted from any flame emission images time-series.

$4.4 \times 4.4 \text{ mm}^2$  for each instantaneous field. The windows size has been varied to ensure the reliability of the results. As previously done for flame imaging, the potential intermittent phenomena are determined by the spectral analysis of the time evolution. This procedure is applied on each operating condition, and the characteristic frequencies obtained for each flame type are presented in Table 2.

Frequency (Hz)		
Flame Type	Flame Imaging	PIV
F1	$70 \pm 3$	$67 \pm 2$
F2	$90 \pm 3$	$91 \pm 2$
F3	---	$130 \pm 2$

**Table 2.** Characteristic frequencies obtained from flame imaging and PIV.

The results show a perfect matching between the frequencies determined by PIV and by flame imaging for both stable F1 and F2 flames. This result points out the strong correlation of the aerodynamics with the periodic flame pocket ejection. As the air velocity

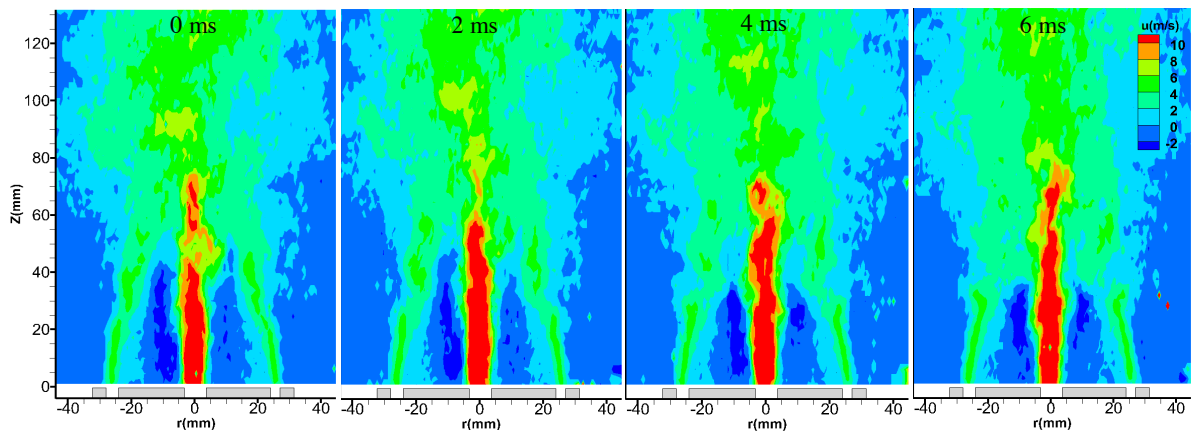


**Figure 9.** Sequence of instantaneous axial velocity fields obtained by 5 kHz PIV (1 over 10 successive fields is shown).

### 5. Time resolved analysis of the aerodynamic structures

A sequence of successive instantaneous velocity fields obtained by PIV is presented Fig. 9. The aerodynamics characteristic frequency is evaluated by extracting and averaging the radial component of the instantaneous velocity in a selected window positioned between the air and methane jets at  $z = 50 \text{ mm}$ ,  $r = 10 \text{ mm}$ . The window area is

increases (F1 to F3), the aerodynamics frequency increases. For the F3 flame, a high frequency is determined on each PIV time series whereas no frequency is obtained on flames images. The flame local detachment, in conditions close to blow-out, does not show any periodicity and the ejection of reactive zone cannot be correlated to aerodynamics structures, for these conditions. Nevertheless, the frequencies obtained from PIV measurements represent the intermittent aerodynamics features of the recirculation zone generated by the annular turbulent flow. The Strouhal number, characterizing the intermittent event of this flow is expressed as:  $St_h = \frac{f \cdot D_b}{U_a}$ , based on the air velocity  $U$ , and bluff-body diameter  $D$ . Flames F1 and F2 presents similar  $St$  number about 0.67. This value can be linked to the natural instability of the annular air jet and corresponds to the jet preferred mode, resulting in the formation of regular vortical rings. Several studies

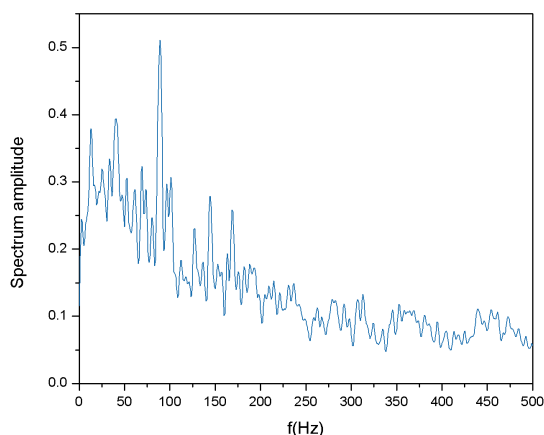


**Figure 8.** FFT profile obtained for the F2 flame.

have also shown that the  $St_c$  corresponding to the preferred mode of the jet lies in the range 0.3-0.8 [13-16]. These vortices, generated at the external base of the annular flow, feed the air driven recirculation zone and interact with the flame tube anchored downstream of the flame leading edge. The strong strain imposed by the vortex interaction on the flame leads to local extinction and periodic pockets ejection. In the case of F3 conditions, flame imaging does not present any characteristic frequency. The ratio  $\frac{f}{U_a}$  and thus the  $St_c$  number, exceeds the value obtained for both F1 and F2 cases. The F3 flame does not seem to be controlled by aerodynamics. Under these conditions, the extinction limit is reached.

### Conclusion

Turbulent Bluff-body flames stabilization phenomena were studied in the present study. The configuration studied is a non-premixed coaxial flow of air and methane. The results show that stabilization of combustion is controlled by the presence of the recirculation zone which induces some periodic ejection of burning pockets allowing ignition of the main trailing flame downstream in the flow. The phenomenon of ejection of flame pockets has a characteristic frequency, which depends on the annular air velocity injection. No specific frequency can be determined for flame close to the extinction limit.

The original flow structure downstream of the Bluff-Body burner is characterized by high-rate PIV. It consists primarily of an internal recirculation area which is defined by two vortices. The first one - a large centripetal vortex - is piloted by the annular air flow and the second one - smaller and centrifugal - is piloted by the central methane jet. Instantaneous velocity periodicity have led to the burning pockets frequency determination which perfectly match with frequency values obtained from high-rate flame imaging for stable flames. This correlation is no more observed for a flame regime close to limit of extinction.

### Acknowledgments

The study is performed in the framework of the 'PASTEC' project with the financial support of ANR (ANR-16-CE22-0005-02)

### References

[1] Beér JM, Chigier NA, Combustion Aerodynamics, Applied Science Publishers Ltd, (1972).

[2] Tong, Y., Liu, X., Wang, Z., Richter, M., & Klingmann, J, Experimental and numerical study on bluff-body and swirl stabilized diffusion flames, *Fuel* 217 (2018) 352–364.

[3] Caetano, N. R., & Silva, L. F., A comparative experimental study of turbulent non premixed flames stabilized by a bluff-body burner, *Experimental Thermal and Fluid Science* 63, (2015) 20-33.

[4] A.R. Masri, R.W. Bilger, Turbulent diffusion flames of hydrocarbon fuels stabilized on a bluff body, *Symp. (Int.) Combust.* 20 (1985) 319.

[5] Susset, K. Mokaddem, D.W. Kendrick, J.C. Rolon, D. Jaffré, D. Honoré, M. Perrin, C. Gray, J.B. Richon, Convenient laser diagnostics for aerodynamic and chemical study of axisymmetric non-premixed Bluff-Body burner flames. In: *Developments in Laser Techniques and Fluid Mechanics. Selected Papers from the 8th International Symposium Lisbon*, 1997.

[6] Susset, M. Trinité, D. Honoré, D. Jaffré, M. Perrin. Experimental investigation of spatio-temporal correlation between aerodynamic and flame front location in an axisymmetric non premixed bluff body burner flame. *Ninth Int. Symposium on Applications of Laser Techniques to Fluid Mechanics*. July 13th-16th, Lisbon, Portugal, 1998.

[7] Mokaddem K., Contribution à la validation expérimentale de deux modèles de combustion turbulente, *Ecole Centrale de Paris*, 1997 Ph.D. Thesis.

[8] Morales, A. J., Lasky, I. M., Geikie, M. K., Engelmann, C. A., & Ahmed, K. A., Mechanisms of flame extinction and lean blowout of bluff body stabilized flames, *Combustion and Flame*, (2019) 203, 31–45.

[9] Nguyen, H. T., Etude expérimentale de l'influence de la géométrie du stabilisateur sur le développement d'une flamme non premlangée, *Ecole Centrale de Lyon*, (1999) Ph. D. Thesis

[10] Esquiva-Dano I., H.T. Nguyen, D. Escudie, Influence of a bluff-body's shape on the stabilization regime of non-premixed flames, *Combust. Flame* 127 (2001) 2167.

[11] Lecordier, B. & Trinite, M., Advanced PIV algorithms with image distortion validation and comparison using synthetic images of turbulent flow/Particle Image Velocimetry: Recent Improvements', *Springer*, (2004) pp. 115-132.

[12] Lecordier, B.; Demare, D.; Vervisch, L. M. J.; Reveillon, J. & Trinite, M., 'Estimation of the accuracy of PIV treatments for turbulent flow studies by direct numerical simulation of multi-phase flow', *Measurement Science and Technology* 12(9), (2001) 1382--1391.

[13] Amélie Danlos, Gildas Lalizel, Béatrice Patte-Rouland. Experimental characterization of the initial zone of an annular jet with a very large diameter ratio. *Experiments in Fluids*, Springer Verlag (Germany), 2013.

[14] Crow SC, Champagne FH. Orderly structure in jet turbulence. *J Fluid Mech* 48, (1971) 547–591

[15] Birbaud AL, Durox D, Ducruix S, Candel S. Dynamics of free jets submitted to upstream acoustic modulations. *Phys Fluids* 19 (2007) (1).

[16] Gutmark E, Ho CM. On the preferred modes and the spreading rate of jets. *Phys Fluids* 26, (1983) 2932–2938